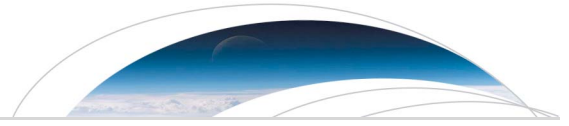




|                  |  |
|------------------|--|
| Title            | Three-dimensional distribution of ionospheric anomalies prior to three large earthquakes in Chile  |
| Author(s)        | He, Liming; Heki, Kosuke   |
| Citation         | Geophysical research letters, 43(14), 7287-7293<br><a href="https://doi.org/10.1002/2016GL069863">https://doi.org/10.1002/2016GL069863</a> |
| Issue Date       | 2016-07-29   |
| Doc URL          | <a href="http://hdl.handle.net/2115/64395">http://hdl.handle.net/2115/64395</a>  |
| Rights           | An edited version of this paper was published by AGU. Copyright 2016 American Geophysical Union  |
| Type             | article  |
| File Information | grl54707.pdf   |



[Instructions for use](#)



## RESEARCH LETTER

10.1002/2016GL069863

## Key Points:

- Preseismic ionospheric TEC anomalies of three Chilean megathrusts
- Simultaneous emergence of the positive and negative anomalies
- Three-dimensional spatial structure of the TEC anomalies

## Supporting Information:

- Supporting Information S1

## Correspondence to:

L. He,  
heliming@mail.neu.edu.cn

## Citation:

He, L., and K. Heki (2016), Three-dimensional distribution of ionospheric anomalies prior to three large earthquakes in Chile, *Geophys. Res. Lett.*, *43*, 7287–7293, doi:10.1002/2016GL069863.

Received 5 JUN 2016

Accepted 1 JUL 2016

Accepted article online 6 JUL 2016

Published online 16 JUL 2016

## Three-dimensional distribution of ionospheric anomalies prior to three large earthquakes in Chile

Liming He<sup>1,2</sup> and Kosuke Heki<sup>2</sup>

<sup>1</sup>Department of Geodesy and Geomatics, School of Resources and Civil Engineering, Northeastern University, Shenyang, China, <sup>2</sup>Department of Earth and Planetary Sciences, Hokkaido University, Sapporo, Japan

**Abstract** Using regional Global Positioning System (GPS) networks, we studied three-dimensional spatial structure of ionospheric total electron content (TEC) anomalies preceding three recent large earthquakes in Chile, South America, i.e., the 2010 Maule ( $M_w$  8.8), the 2014 Iquique ( $M_w$  8.2), and the 2015 Illapel ( $M_w$  8.3) earthquakes. Both positive and negative TEC anomalies, with areal extent dependent on the earthquake magnitudes, appeared simultaneously 20–40 min before the earthquakes. For the two midlatitude earthquakes (2010 Maule and 2015 Illapel), positive anomalies occurred to the north of the epicenters at altitudes 150–250 km. The negative anomalies occurred farther to the north at higher altitudes 200–500 km. This lets the epicenter, the positive and negative anomalies align parallel with the local geomagnetic field, which is a typical structure of ionospheric anomalies occurring in response to positive surface electric charges.

### 1. Introduction

Ionospheric total electron contents (TECs), derived by comparing phases of two L band microwave signals from Global Positioning System (GPS) satellites, allow us to study earthquakes from unique points of view. Coseismic ionospheric disturbances sometimes provide information on rupture processes of earthquakes [e.g., Heki *et al.*, 2006]. Their amplitudes depend on moment magnitudes ( $M_w$ ) of earthquakes [Cahyadi and Heki, 2015], and ionospheric monitoring may contribute to early warning of tsunami arrivals [e.g., Astafyeva *et al.*, 2013].

Apart from these coseismic disturbances, Heki [2011] found ionospheric electron enhancements starting ~40 min before the 2011 Tohoku-oki earthquake ( $M_w$  9.0), Japan, using a dense array of continuous GPS stations. Through debates between critical papers [Kamogawa and Kakinami, 2013; Utada and Shimizu, 2014; Masci *et al.*, 2015] and replies to them [Heki and Enomoto, 2013, 2014, 2015], Heki and Enomoto [2015] showed that the enhancements preceded eight past earthquakes with  $M_w$  8.2 or more. They found that the enhancements started about 20/40 min prior to  $M_w$  8/9 earthquakes and that the changes in vertical TEC (VTEC) rates depend on  $M_w$  as well as background absolute VTEC. Although similar changes often occur due to geomagnetic activities, Heki and Enomoto [2015] demonstrated that they are not frequent enough to account for the observed preseismic anomalies. The reader is referred to the introduction of Heki and Enomoto [2015] for the history of the arguments.

These past papers mainly focused on the reality of enhancements and their significance among space weather origin disturbances, and little discussed spatial structures and areal extents of the anomalies. Here we study three-dimensional (3-D) structures of preseismic ionospheric anomalies, in order to shed light on the underlying physical processes. We focus on three recent large interplate earthquakes in Chile, South America, i.e., the 2010 Maule ( $M_w$  8.8), the 2014 Iquique ( $M_w$  8.2), and the 2015 Illapel ( $M_w$  8.3) earthquakes. Large number of continuous GPS stations distributed over South America make this region ideal for such studies.

### 2. GPS Data and TEC Analysis Procedures

#### 2.1. The Three Chilean Earthquakes

In this study, we analyzed the behaviors of ionospheric TEC before and after the three large earthquakes in Chile using regional GPS data (Figure 1). The 27 February 2010 Maule earthquake ruptured the boundary between the Nazca and the South America Plates known as the Constitución-Concepción seismic gap in

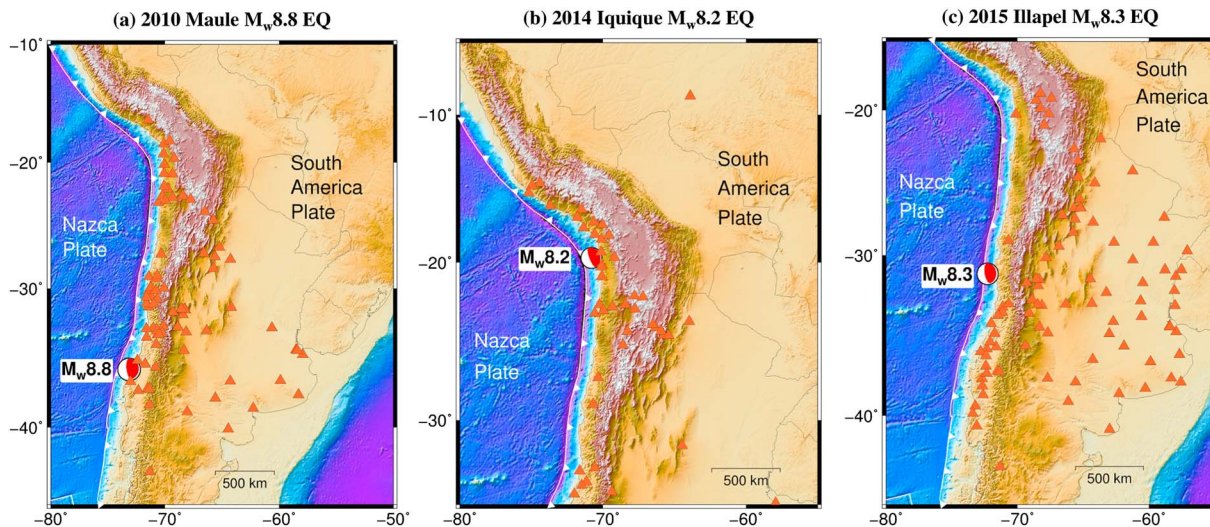


**Figure 1.** GPS stations (red triangles) used to study the three Chilean earthquakes, (a) 83 stations for the 2010 Maule, (b) 47 stations for the 2014 Iquique, and (c) 91 stations for the 2015 Illapel earthquakes. The beach balls show the epicenters and focal mechanisms.

Central Chile [Madariaga *et al.*, 2010]. The 1 April 2014 Iquique earthquake ruptured the same plate boundary around the Peru-Chile border [Ruiz *et al.*, 2014]. The 16 September 2015 Illapel earthquake occurred in a segment  $\sim 500$  km north of the Maule earthquake [Ye *et al.*, 2016]. Geographic latitudes of their epicenters are  $36.1^{\circ}\text{S}$ ,  $19.6^{\circ}\text{S}$ , and  $31.6^{\circ}\text{S}$ , respectively, and their geomagnetic latitudes are lower by  $\sim 10^{\circ}$ . The Maule earthquake occurred past midnight (03:34:14) in local time (LT) and the other two occurred in the evening, i.e., at 20:46:47 LT (2014 Iquique) and at 19:54:33 LT (2015 Illapel).

## 2.2. GPS-TEC Data Processing

We first obtained slant TEC (STEC), number of electrons integrated along the travel path of microwave signals, and removed the phase ambiguities by letting the TEC time series derived by carrier phases align with those by pseudoranges [Calais and Minster, 1995; Mannucci *et al.*, 1998]. The STEC data still include satellite and receiver interfrequency biases (IFBs). We obtained the satellite IFBs from the header information of global ionospheric maps available from University of Berne, Switzerland [Schaer *et al.*, 1998]. We inferred the receiver IFBs by minimizing the scatter of nighttime VTEC at individual stations [Rideout and Coster, 2006].

After removing IFBs, we calculated the absolute VTEC by multiplying the STEC with the cosine of the incident angle of the line of sight with a thin shell at 300 km above the ground (In drawing sub-ionospheric points (SIPs) in Figures 2 and 3, we assumed different heights). We use VTEC throughout this study because they are free from apparent variations due to changing satellite elevations. Geomagnetic activities were low when the 2010 Maule and the 2014 Iquique earthquakes occurred but were moderately high during the 2015 Illapel earthquake (Figure S1 in the supporting information).

We followed Heki and Enomoto [2015] to identify bends (breaks) in VTEC before earthquakes using the Akaike's information criterion (AIC) (Figure S2). Figure 2 shows VTEC time series observed using different pairs of GPS satellites (marked by their unique pseudo random noise (PRN) numbers) and receivers over 2–3 h intervals including the three Chilean earthquakes. We modeled the VTEC curves with the polynomials of time with degrees 3–5, excluding the intervals from the onsets of the anomalies detected using AIC to 20 min after the earthquakes. We define positive and negative departures from the models as anomalous increases (enhancements) and decreases of VTEC, respectively.

Some stations show clear coseismic disturbances, e.g., CRZL-PRN20, AREQ-PRN01, and TILC-PRN14, in Figures 2a, 2b, and 2c, respectively. Such disturbances clearly appear where SIPs and stations are on the northern side of the epicenter, owing to interaction with geomagnetic fields [Rolland *et al.*, 2013]. Coseismic electron depletions are clear above the regions of large vertical coseismic crustal movements [Shinagawa *et al.*, 2013], e.g., RCSD-PRN23, LYAR-PRN23, and CMPN-PRN24, in Figures 2a–2c, respectively, but are smaller outside such regions.

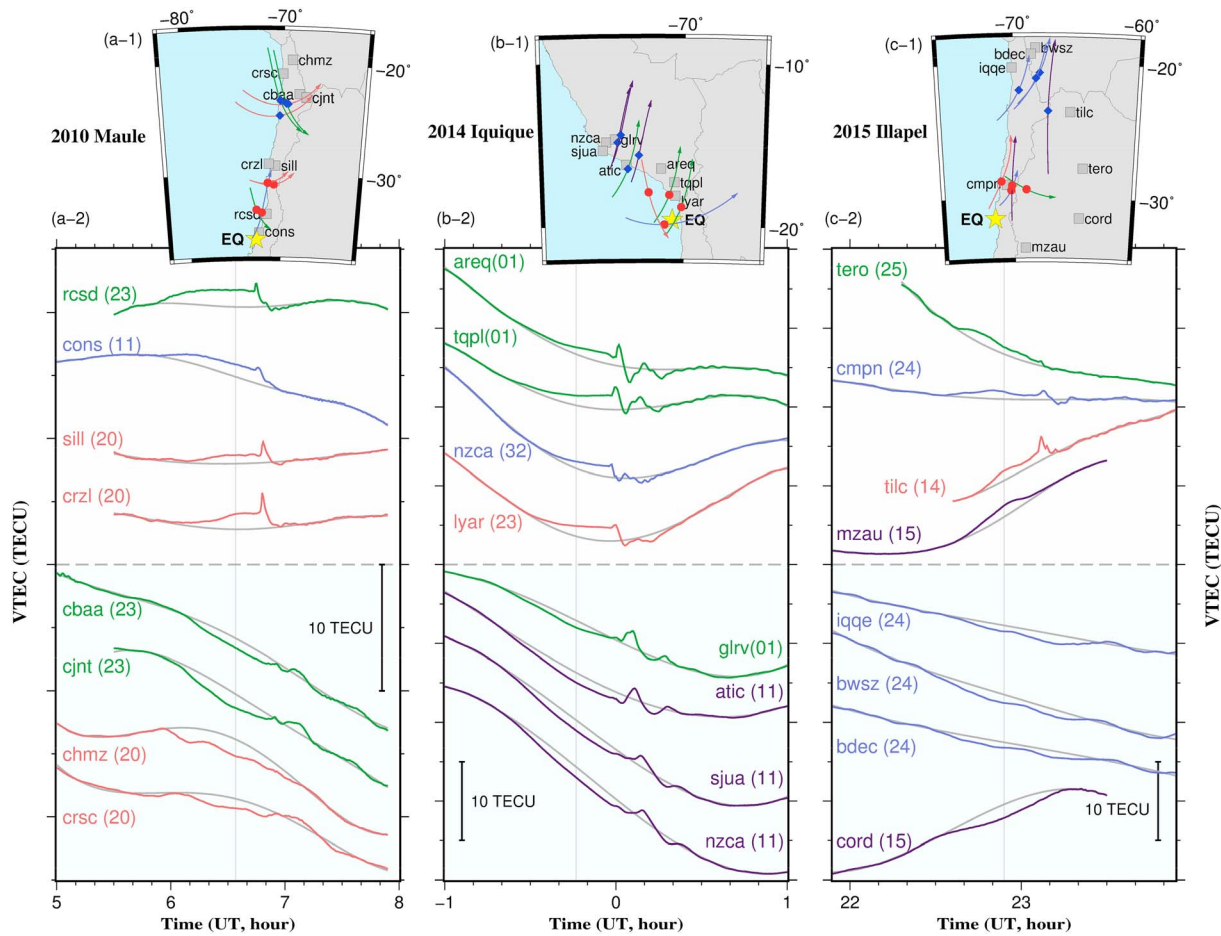


**Figure 2.** The VTEC time series observed with eight pairs of station-satellite (same colors for same satellites) showing preseismic enhancements and decreases shown in the upper and lower halves, respectively. The gray curves are the reference models, from which we define VTEC anomalies shown in Figure 3. The vertical gray lines indicate earthquake occurrence times. The maps at the top show the positions of GPS stations (gray squares) and the SIP trajectories (red dots and blue diamonds indicate the earthquake times for stations showing enhancements and decreases, respectively) over the studied intervals. We assumed 200 and 400 km for ionospheric heights in drawing SIP tracks for enhancements and decreases, respectively. The yellow stars show the epicenters.

Preseismic TEC enhancements emerge ~40 min before the 2010 Maule earthquake (Figure 2a-2, upper half). We found that TEC starts to decrease (Figure 2a-2, lower half) simultaneously at stations farther to the north of the epicenter. The 2014 Iquique (Figure 2b-2) and 2015 Illapel (Figure 2c-2) earthquakes also showed similar sets of VTEC enhancements and decreases starting ~20 min before earthquakes.

### 3. Preseismic TEC Anomalies of the Three Chilean Earthquakes

Figure 3 shows map distributions of the TEC anomalies at three time epochs, i.e., 30 min, 15 min, and immediately (30 s) before the 2015 Illapel earthquake. The dots represent the SIP positions calculated assuming the ionospheric heights of ~170 km and ~420 km, for positive and negative TEC anomalies, respectively. SIP coordinates depend on the assumed height of an ionospheric anomaly, and multiple SIPs obtained with different satellite-station pairs are expected to converge when the assumed anomaly height is correct (Figure S3). In order to constrain the altitudes of the observed positive and negative anomalies, we tuned their altitudes so that they minimize the angular standard deviations of the SIPs of positive and negative groups, respectively (Figure S4).

No anomalies exist 30 min before the earthquake (Figures 3a and 3d). Both positive and negative VTEC anomalies have already emerged to the north of the epicenter ~15 min before the earthquake (Figures 3b and 3e). They become the largest immediately before the earthquake (Figures 3c and 3f). Such positive and negative TEC anomalies also preceded the 2010 Maule (Figure S5) and the 2014 Iquique (Figure S6)

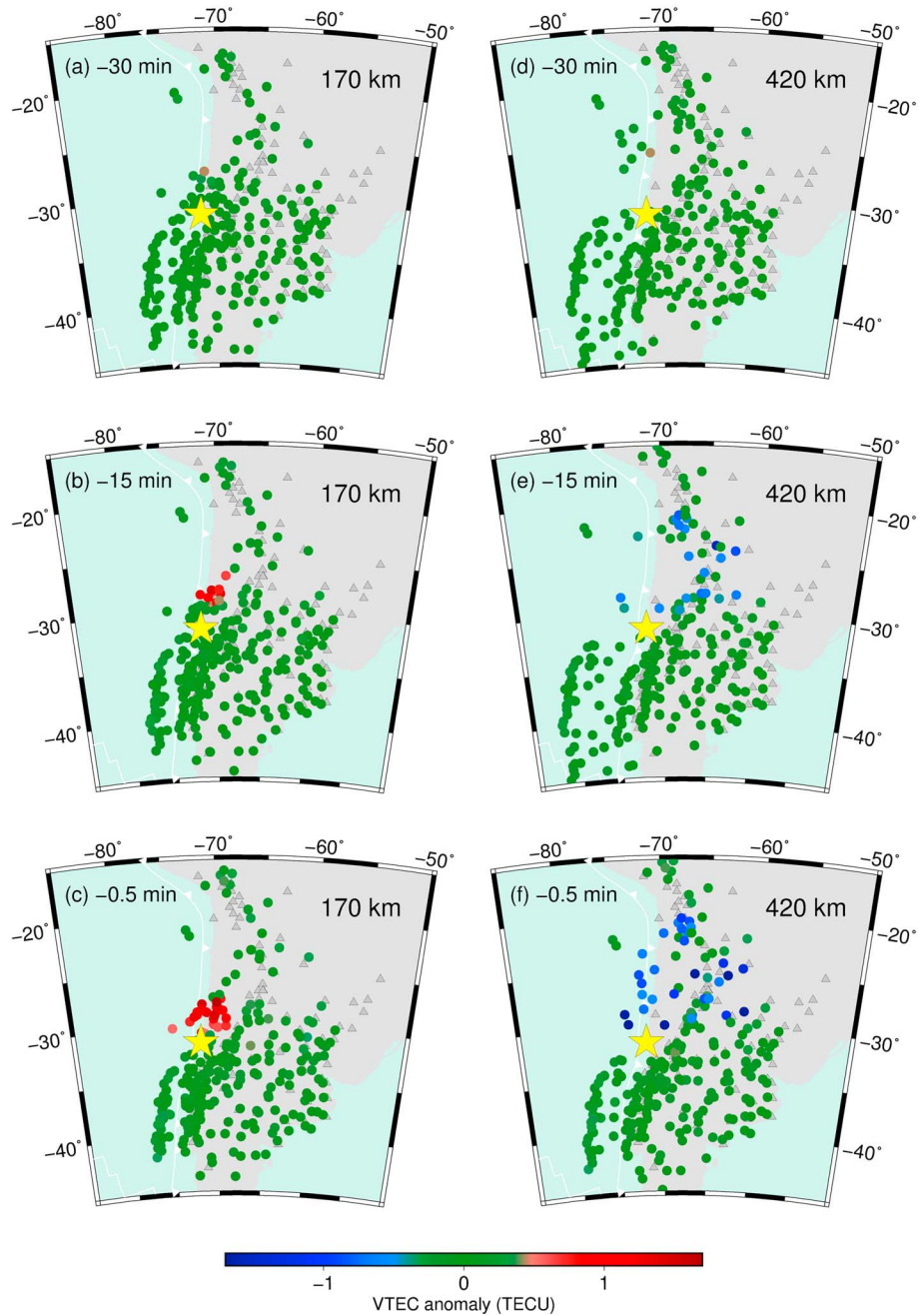


**Figure 3.** Distribution of SIPs showing preseismic positive/negative VTEC anomalies at (a, d) 30 min, (b, e) 15 min, and (c, f) 0.5 min before the 2015 Illapel earthquake. We used five GPS satellites (PRN12, 14, 15, 24, and 25). We derived the SIP positions in Figures 3a–3c and 3d–3f assuming the ionospheric heights of 170 and 420 km, respectively. The yellow star shows the epicenter, and gray triangles indicate GPS receivers. We removed negative ( $< -0.5$  TECU) and positive ( $> +0.5$  TECU) anomalies from Figures 3a–3c and 3d–3f, respectively, for visual clarity.

earthquakes. For the 2010 and 2015 events, the positive anomalies are located just to the north of the epicenters, and the negative anomalies appeared far to the north over a larger area. We find fewer anomalies to the south of the epicenter. For the 2014 event, the positive anomalies emerged just above the epicenter, and the negative anomalies appeared both on the northern and southern sides.

Figure 4 compares the map views of preseismic positive VTEC anomalies immediately before the three Chilean earthquakes. We tuned the ionospheric heights to minimize the scatters of the positive anomalies (Figure S4). The dimensions of areas of positive VTEC anomalies depend on  $M_w$  (hence on fault size); the

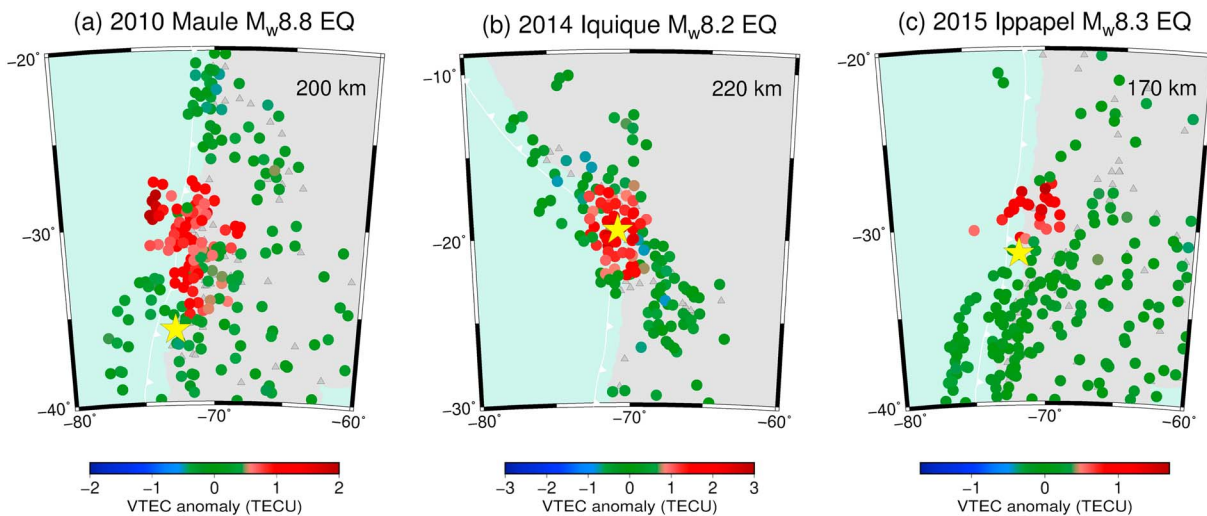


**Figure 4.** Preseismic VTEC enhancements 0.5 min before the (a) 2010 Maule, (b) 2014 Iquique, and (c) 2015 Illapel earthquakes. We assumed the ionospheric altitudes of 200, 220, and 170 km in calculating SIP positions for the three earthquakes, respectively. The yellow stars show the epicenters. The gray triangles represent the positions of GPS receivers.

anomaly of the 2010  $M_w$  8.8 Maule earthquake is larger than the other two ( $M_w$  8.2 and 8.3) earthquakes. The background VTEC, on the other hand, does not seem to influence the dimension; the background VTEC of the 2014 Iquique earthquake was  $>10$  times as large as that of the 2010 Maule earthquake [see Heki and Enomoto, 2015, Figure 1].

## 4. Discussions

### 4.1. Onset Time and the VTEC Rate Changes

Before discussing 3-D spatial distribution of the ionospheric anomalies, we briefly discuss other aspects of the anomalies. Using multiple pairs of satellites and stations, we found that the onset times of the anomalies were  $\sim 40$ ,  $\sim 23$ , and  $\sim 22$  min before the 2010, 2014, and 2015 earthquakes (Figure S2), respectively. This is consistent with other earthquakes [Heki and Enomoto, 2015, Figure 5a].

Heki and Enomoto [2015] have already used the 2010 Maule and 2014 Iquique earthquakes to derive the empirical relationship (equation (5)) between the background VTEC, VTEC rate changes, and  $M_w$ . This equation assumes that magnitudes of very large earthquakes are already determined in the nucleation stage. The observations suggest that cascading up would not much exceed the difference between the predicted and real magnitudes [0.28 in Heki and Enomoto, 2015]. For the 2015 Illapel event, a new earthquake, the background VTEC of 22 total electron content unit (TECU),  $1 \text{ TECU} = 10^{16} \text{ el m}^{-2}$  and the observed break of 4.3 TECU/h (CMPN-PRN24) predict  $M_w$  of 8.7. This is 0.4 larger than the actual  $M_w$ . Inclusion of this new event, and future large earthquakes, would further refine the coefficients of the equation and improve the accuracy of the expected  $M_w$ .

### 4.2. Spatial Structures of Preseismic Ionospheric Anomalies

For studying 3-D spatial distribution of the TEC anomalies, we use the data of the 2015 Illapel earthquake, for which the station distribution is the most suitable (Figure 1). The conventional way is to map horizontal distribution of TEC anomalies, like Figure 3, as if they occurred on a horizontal plane at a certain height. In Figure 5a, we drew a “longitudinal profile,” where we plot the calculated heights and latitudes of the intersections of the line-of-sight vectors with the 70 W meridional plane. Because the line of sights need to intersect with the plane at high angles, we used only PRN14 and 25. The profile shows that the positive and negative anomalies line up along the magnetic field (inclination  $-32^\circ$ ) [Thebault et al., 2015] from the bottom of ionosphere ( $\sim 85$  km high) above the epicenter.

Figures 3 and 5a suggest the 3-D spatial structure of the preseismic ionospheric anomalies as illustrated in Figure 5b. This resembles to the numerical calculation results of the ionospheric response to the positive

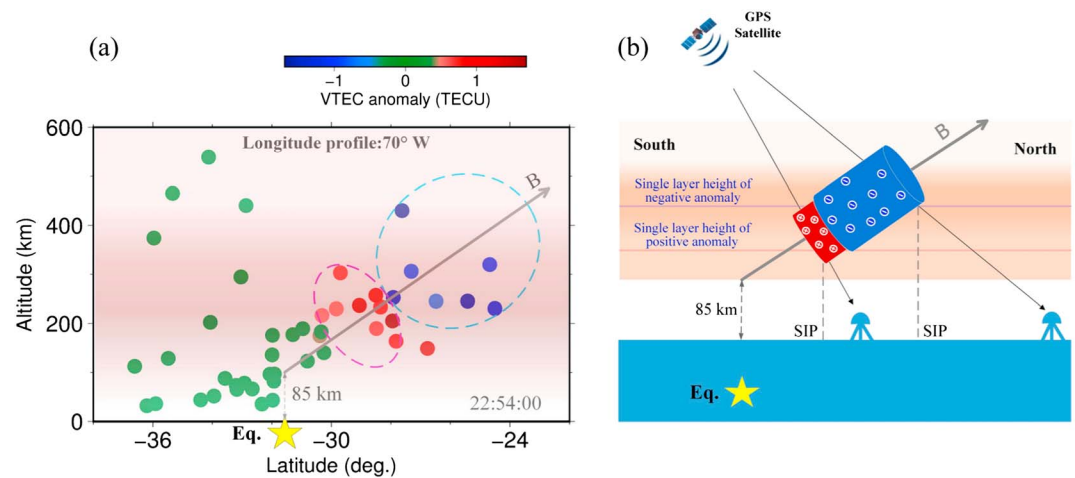


**Figure 5.** (a) Longitudinal profile at 70°W of VTEC anomalies immediately before the 2015 Illapel earthquake drawn using PRN 14 and 25. We show latitudinal profile in Figure S7. (b) Schematic illustration showing the 3-D distribution of positive and negative anomalies. A thick gray arrow shows the geomagnetic field. The red and the blue regions show the positive and negative electron density anomalies. The yellow stars show the epicenter.

surface electric charges [see *Kuo et al.*, 2014, Figure 12e]. For the 2010 Maule earthquake, the distribution of GPS stations (Figure 1a) was not good enough to plot the longitudinal profiles, but the SIP maps (Figure S5) do suggest a similar 3-D structure. In the 2014 Iquique earthquake, the negative anomalies exist on both the north and south of the positive anomalies (Figure S6). This difference might reflect the lower geomagnetic latitude ( $\sim 10^\circ\text{S}$ ) of the 2014 earthquake epicenter. We are also preparing for a systematic search for the mirror image anomalies that are expected to emerge at geomagnetic conjugate points.

#### 4.3. Physical Process Responsible for Preseismic TEC Anomalies

*Kuo et al.* [2014] demonstrated, with numerical simulation, that the westward electric field in the ionosphere originated from the upward atmospheric electric current causes obliquely downward  $\mathbf{E} \times \mathbf{B}$  drift of electrons. This drift causes the increase and decrease of electron density at altitudes of  $\sim 200$  and  $\sim 400$  km, respectively, and results in the positive and negative anomalies lying along the geomagnetic field. The observed anomalies before the 2015 Illapel earthquake (Figure 5) are consistent with this picture. The nighttime ionosphere before this earthquake is changed by  $\sim 10\%$  of the background VTEC. This requires the maximum density of  $\sim 10 \text{ nA m}^{-2}$  of upward atmospheric electric current at the geomagnetic latitude ( $21.7^\circ\text{S}$ ) of the 2015 Illapel earthquake [*Kuo et al.*, 2014].

A candidate mechanism to explain such currents is the outflow of positive holes from fast stressed rock to unstressed rock observed in laboratory experiments [e.g., *Freund et al.*, 2009]. Such currents sharply increase immediately before the failure of rock samples and then decrease exponentially over a short time after the failure. This resembles the observed VTEC anomaly behaviors. Although there are no decisive evidences, the present observations support the scenario that positive charges from rocks under near-failure stress, possibly in the earthquake nucleation stage, cause ionospheric anomalies immediately before large earthquakes.

#### Acknowledgments

We thank two reviewers for constructive comments. L.H. was supported by the China Scholarship Council (CSC) and by the National Natural Science Foundation of China (41104104). The Chilean GNSS data for the 2010 Maule earthquake were provided by C. Vigny (ENS). We downloaded the Argentine (RAMSAC/IGNA) and Brazilian (RBMC/IBGE) GNSS data from their official webpages. We downloaded additional data from IGS ([www.igs.org](http://www.igs.org)) and UNAVCO ([www.unavco.org](http://www.unavco.org)). We thank C. L. Kuo, National Central University, Taiwan, for validating the observation results using the simulation model developed in his group.

#### References

- Astafyeva, E., L. Rolland, P. Lognonné, K. Khelifi, and T. Yahagi (2013), Parameters of seismic source as deduced from 1 Hz ionospheric GPS data: Case study of the 2011 Tohoku-oki event, *J. Geophys. Res. Space Physics*, *118*, 5942–5950, doi:10.1002/jgra.50556.
- Calais, E., and J. B. Minster (1995), GPS detection of ionospheric perturbations following the January 17, 1994, Northridge earthquake, *Geophys. Res. Lett.*, *22*, 1045–1048, doi:10.1029/95GL00168.
- Cahyadi, M. N., and K. Heki (2015), Coseismic ionospheric disturbance of the large strike-slip earthquakes in North Sumatra in 2012:  $M_w$  dependence of the disturbance amplitudes, *Geophys. J. Int.*, *200*, 116–129.
- Freund, F. T., I. G. Kulahci, G. Cyr, J. Ling, M. Winnick, J. Tregloan-Reed, and M. M. Freund (2009), Air ionization at rock surfaces and pre-earthquake signals, *J. Atmos. Sol. Terr. Phys.*, *71*, 1824–1834, doi:10.1016/j.jastp.2009.07.013.
- Heki, K. (2011), Ionospheric electron enhancement preceding the 2011 Tohoku-Oki earthquake, *Geophys. Res. Lett.*, *38*, L17312, doi:10.1029/2011GL047908.
- Heki, K., and Y. Enomoto (2013), Preseismic ionospheric electron enhancements revisited, *J. Geophys. Res. Space Physics*, *118*, 6618–6626, doi:10.1002/jgra.50578.

- Heki, K., and Y. Enomoto (2014), Reply to comment by K. Heki and Y. Enomoto on "Preseismic ionospheric electron enhancements revisited", *J. Geophys. Res. Space Physics*, *119*, 6016–6018, doi:10.1002/2014JA020223.
- Heki, K., and Y. Enomoto (2015),  $M_w$  dependence of the preseismic ionospheric electron enhancements, *J. Geophys. Res. Space Physics*, *120*, 7006–7020, doi:10.1002/2015JA021353.
- Heki, K., Y. Otsuka, N. Choosakul, N. Hemmakorn, T. Komolmis, and T. Maruyama (2006), Detection of ruptures of Andaman fault segments in the 2004 Great Sumatra Earthquake with coseismic ionospheric disturbances, *J. Geophys. Res.*, *111*, B09313, doi:10.1029/2005JB004202.
- Kamogawa, M., and Y. Kakinami (2013), Is an ionospheric electron enhancement preceding the 2011 Tohoku-oki earthquake a precursor?, *J. Geophys. Res. Space Physics*, *118*, 1751–1754, doi:10.1002/jgra.50118.
- Kuo, C. L., L. C. Lee, and J. D. Huba (2014), An improved coupling model for the lithosphere-atmosphere-ionosphere system, *J. Geophys. Res. Space Physics*, *119*, 3189–3205, doi:10.1002/2013JA019392.
- Madariaga, R., M. Métois, C. Vigny, and J. Campos (2010), Central Chile finally breaks, *Science*, *328*, 181–182.
- Mannucci, A., B. Wilson, D. Yuan, C. Ho, U. Lindqwister, and T. Runge (1998), A global mapping technique for GPS-derived ionospheric total electron content measurements, *Radio Sci.*, *33*, 565–582, doi:10.1029/97RS02707.
- Masci, F., J. N. Thomas, F. Villani, J. A. Secan, and N. Rivera (2015), On the onset of ionospheric precursors 40 min before strong earthquakes, *J. Geophys. Res. Space Physics*, *120*, 1383–1393, doi:10.1002/2014JA020822.
- Rideout, W., and A. Coster (2006), Automated GPS processing for global total electron content data, *GPS Solut.*, *10*, 219–228.
- Rolland, L. M., M. Vergnolle, J. M. Nocquet, A. Sladen, J. X. Dessa, F. Tavakoli, H. R. Nankali, and F. Cappa (2013), Discriminating the tectonic and non-tectonic contributions in the ionospheric signature of the 2011,  $M_w$  7.1, dip-slip Van earthquake, Eastern Turkey, *Geophys. Res. Lett.*, *40*, 2518–2522, doi:10.1002/grl.50544.
- Ruiz, S., M. Métois, A. Fuenzalida, J. Ruiz, F. Leyton, R. Grandin, C. Vigny, R. Madariaga, and J. Campos (2014), Intense foreshocks and a slow slip event preceded the 2014 Iquique  $M_w$  8.1 earthquake, *Science*, *345*, 1165–1169.
- Schaer, S., W. Gurtner, and J. Feltens (1998), IONEX: The ionosphere map exchange format version 1, in *Proceedings of the IGS AC workshop*, Darmstadt, Germany.
- Shinagawa, H., T. Tsugawa, M. Matsumura, T. Iyemori, A. Saito, T. Maruyama, H. Jin, M. Nishioka, and Y. Otsuka (2013), Two-dimensional simulation of ionospheric variations in the vicinity of the epicenter of the Tohoku-Oki earthquake on 11 March 2011, *Geophys. Res. Lett.*, *40*, 5009–5013, doi:10.1002/2013GL057627.
- Thebault, E., et al. (2015), International geomagnetic reference field: The 12<sup>th</sup> generation, *Earth Planets Space*, *67*, 1–19.
- Utada, H., and H. Shimizu (2014), Comment on "Preseismic ionospheric electron enhancements revisited" by K. Heki and Y. Enomoto, *J. Geophys. Res. Space Physics*, *119*, 6011–6015, doi:10.1002/2014JA020044.
- Ye, L., T. Lay, H. Kanamori, and K. D. Koper (2016), Rapidly estimated seismic source parameters for the 16 September 2015 Illapel, Chile  $M_w$  8.3 earthquake, *Pure Appl. Geophys.*, *173*, 321–332.